Kearsley, A T, Colaux, J L, Ross, D K, Wozniakiewicz, Penelope J., Gerlach, L, Anz-Meador, P, Griffin, T, Reed, B, Opiela, J, Palitsin, V V and others
(2017) *Hypervelocity impact in low earth orbit: finding subtle impactor signatures on the Hubble Space Telescope.* Procedia Engineering, 204 . pp. 492-499. ISSN 1877-7058.

Versions of research works

Versions of Record

If this version is the version of record, it is the same as the published version available on the publisher's web site. Cite as the published version.

Author Accepted Manuscripts

If this document is identified as the Author Accepted Manuscript it is the version after peer review but before type setting, copy editing or publisher branding. Cite as Surname, Initial. (Year) 'Title of article'. To be published in *Title of Journal* , Volume and issue numbers [peer-reviewed accepted version]. Available at: DOI or URL (Accessed: date).

Enquiries

If you have questions about this document contact ResearchSupport@kent.ac.uk. Please include the URL of the record in KAR. If you believe that your, or a third party's rights have been compromised through this document please see our Take Down policy (available from https://www.kent.ac.uk/guides/kar-the-kent-academic-repository#policies).

14th Hypervelocity Impact Symposium 2017, HVIS2017, 24-28 April 2017, Canterbury, Kent, UK

Hypervelocity impact in low earth orbit: finding subtle impactor signatures on the Hubble Space Telescope.

A T Kearsley[a,b,c*], J L Colaux[d,†] D K Ross[e], P J Wozniakiewicz[b,c], L Gerlach[f], P Anz-Meador[g], T Griffin[h], B Reed[h], J Opiela[g], V V Palitsin[d], G W Grime[d], R P Webb[d], C Jeynes[d], J Spratt[b], T Salge[b], M J Cole[c], M C Price[c] and M J Burchell[c].

[a] Dunholme, Raven Hall Road, Ravenscar, YO13 0NA, UK;
[b] Natural History Museum (NHM, retired), Cromwell Road, London, UK.
[c] School of Physical Sciences, University of Kent, Canterbury, Kent, UK.
[d] Ion Beam Centre (IBC), University of Surrey, Guildford, UK.
[e] UTEP, Jacobs-JETS, and NASA Johnson Space Center (NASA-JSC), Houston, TX, USA.
[f] European Space Agency (ESA, retired), Noordwijk, The Netherlands.
[g] NASA Goddard Space Flight Center (GSFC), Greenbelt, Maryland, USA.

Abstract

Return of materials from the Hubble Space Telescope (HST) during shuttle orbiter service missions has allowed inspection of large numbers of hypervelocity impact features from long exposure at about 615 km altitude in low Earth orbit (LEO) [1,2]. Here we describe the application of advanced X-ray microanalysis techniques on scanning electron microscopes (SEM), microprobes and a 2 MV Tandetron, to nearly 400 impacts on the painted metal surface of the Wide Field and Planetary Camera 2 (WFPC2) radiator shield [3,4]. We identified artificial Orbital Debris (OD) and natural Micrometeoroid (MM) origins for small [5] and even for larger particles [6], which usually may leave little or no detectable trace on HST solar arrays, as they penetrate through the full cell thickness [2,7].

Keywords: Hubble Space Telescope; orbital debris; micrometeoroids; microanalysis

* Corresponding author. Tel.: +44-774-8186753.
E-mail address: kearsleys@runbox.com.
† J L Colaux is now at Synthesis, Irradiation, and Analysis of Materials (SIAM), Department of Physics, University of Namur, Belgium

1. Introduction

SEM and energy dispersive X-ray microanalysis (EDX) have long been used to try to find LEO impact residues [e.g. 8]. Recent advances in high count rate silicon drift (SDD) and annular pole-piece detectors now allow rapid mapping, and identification of impactors using SEM and particle induced X-ray emission (PIXE) [9, 10].

2. Methods

2.1 Sample preparation, analytical instruments and techniques

Core samples were cut from the 0.8 x 2.2 m radiator shield [4] and examined in two SEM instruments: Zeiss EVO 15LS at the Natural History Museum (NHM) and JEOL 7600F (field emission) at NASA-JSC, both fitted with inclined SDD EDX detectors. A Cameca SX100 wavelength dispersive (WDX) microprobe, and a large-area SDD detector pole-piece mounted on FEI Quanta 650 field emission SEM at NHM were also used. If no unambiguous chemical contribution was revealed, the Ion Beam Centre (IBC) 2.5 MeV proton beam was employed for PIXE [10].

At NHM we collected EDX spectra for 200 seconds, with accelerating voltage of 20 kV and electron beam current of 3 nA. Oxford Instruments INCA software separated peak and background X-ray counts for K emission lines. Knowing likely OD and MM signature elements/assemblages [2], and pristine WFPC paint and alloy compositions (Fig. 1), we extracted data for: Mg, Al, Si, S, K, Ca, Ti, Cr, Mn, Fe, Ni, Cu and Zn. Recognition of each element in the spectra was by the accepted microanalysis convention, i.e. the element was 'detected' when characteristic X-ray peak area exceeded variation in background X-ray counts by a factor of 3. Complex surface shape in the impact features, and variability of porosity and matrix composition in frozen impact melt prevented quantitative correction for secondary X-ray fluorescence and absorption, and weight percentage values were therefore not calculated. Depth models and profiles were made from stereo-pair Backscattered Electron Images (BEI) of impact features.

2.2 Experimental analogues

A light gas gun (LGG) shot at White Sands Test Facility fired projectiles onto a surface similar to that of WFPC2. Melted residue was located quickly by BEI and SEM-EDX mapping, validating this combination of techniques. Further shots at the University of Kent [11] used 'buck-shot' of olivine, pyrrhotite, iron, aluminium and corundum at ~ 6 km/s. These MM and OD analogues let us test appropriate imaging and analysis protocols for WFPC2 data.

3. Results

A polished cross section revealed complex composition of the surface paint (Fig. 1), penetration through this layer might mobilize Al alloy (including Mg and Fe-bearing inclusions), if shallower it would only sample paint.
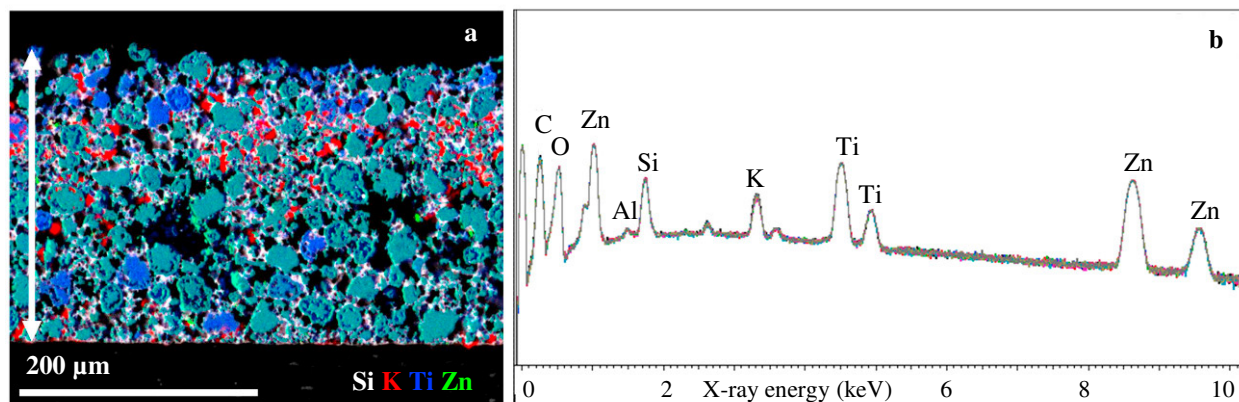

Fig. 1. SEM-EDX of section through WFPC2 paint: a) maps; b) 10 spectra, note that Mg and Fe are not seen.

In > 50% of the small craters analysed at NHM [5], frothy impact melt immediately showed elements from paint (O, Si, S, K, Ti and Zn), and a clear excess of Mg and Fe, with little or no Al (e.g. Fig. 2). A few also contained: Ca (with Mg and Fe); Cr (with Fe and S) or Ni (with Fe). One contained excess Al without Fe or Mg (Fig. 3).
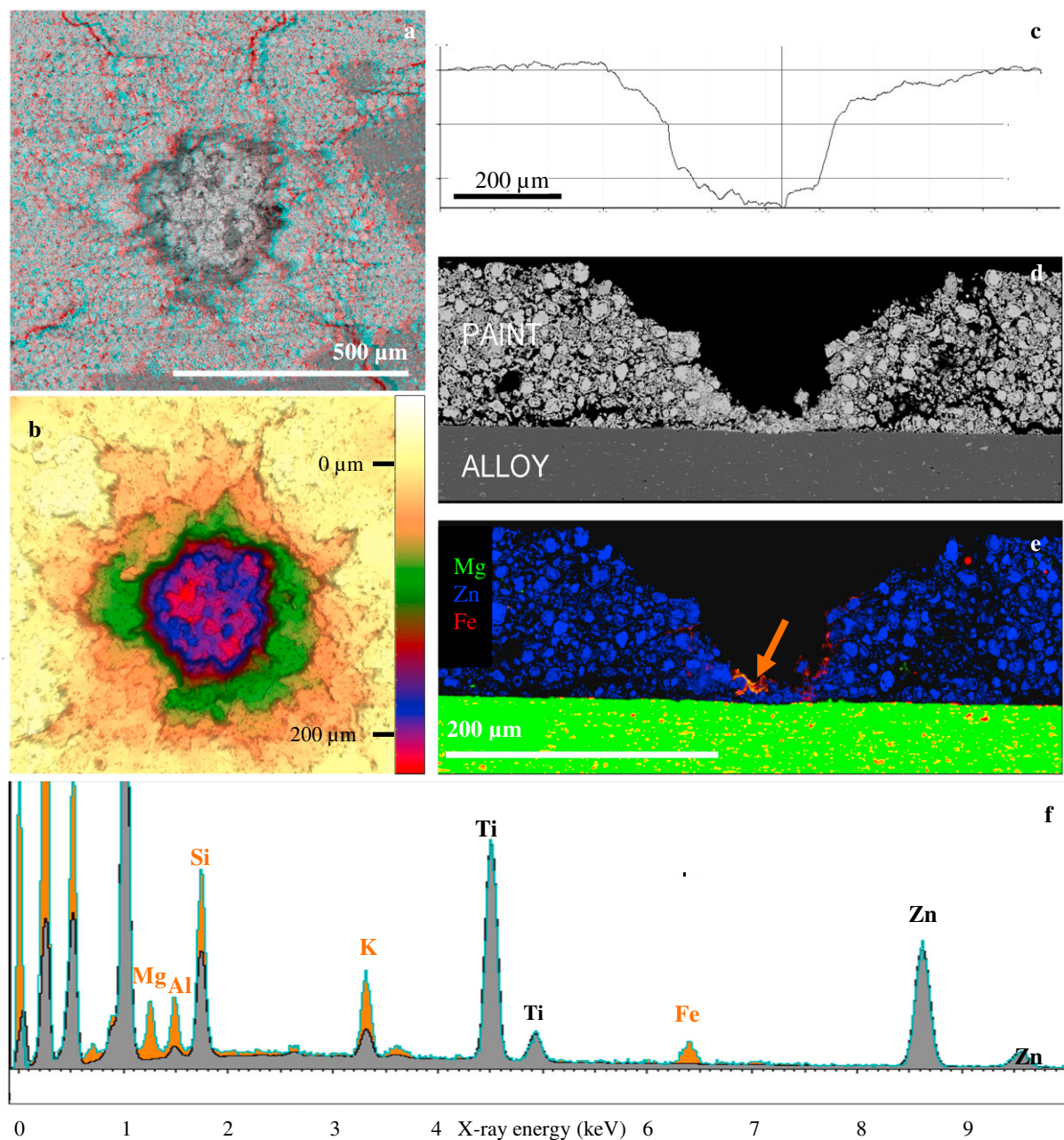

Fig. 2. Small impact feature WFPC2-11: a) stereo BEI anaglyph; b) depth model; c) profile; d) BEI and e) WDX maps of a polished vertical section, revealing Mg and Fe-rich residue (arrowed); f) SEM-EDX spectrum (orange) from arrowed location in maps (e), shows high Mg/Al when compared to spectrum of neighbouring paint area (grey), Mg therefore cannot be derived from the underlying alloy, and must (with Fe) be from the impacted particle.
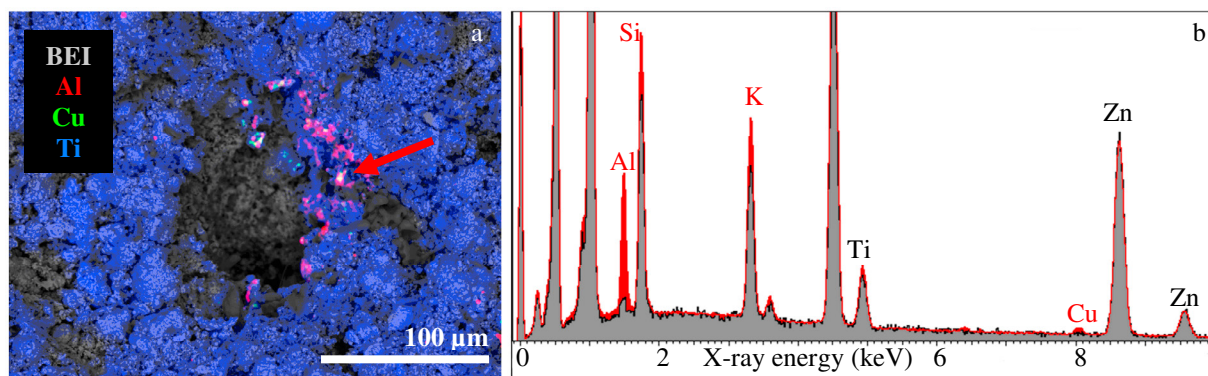
Fig. 3. Small impact WFPC2-380: a) BEI and SEM-EDX maps show Al and Cu around crater; b) spectrum of frothy melt lining the crater (red, arrowed) shows Al enrichment compared to surrounding area of paint (grey spectrum).

Larger impact features [6] showed detachment of paint and a bowl-shaped pit or overlapping pits in exposed alloy – with a variable quantity of frothy paint-rich and metal-rich frozen melt. Repeated long duration (200 secs) SEM-EDX spectra were required to find subtle signs of extraneous elements in many features, both large and small. PIXE and WDX mapping showed patches with obvious extraneous elements, including Fe, Ni metal.

3.1 Subtle impactor traces

3.1.1 Smaller impacts, restricted to the paint layer (e.g. Fig. 4).

Clean zinc orthotitanate (ZOT) paint shows very low Mg and Fe (Fig. 1b), usually below or close to detection limit. To recognize low concentrations of Mg and/or Fe in small features, we plotted their X-ray counts as a function of their detection limits [9], with a threshold of Al < 6 % of total X-ray counts to separate spectra that might contain contamination from alloy. LGG test shots of olivine [11], gave spectra with Mg and Fe residue across a wide range of impactor concentration (Fig. 4, open squares), clearly higher than clean ZOT paint (Fig. 4, blue points). This type of plot gave a positive identification of impactor composition in over 40 WFPC2 features (e.g. WFPC2-339, Fig. 4).
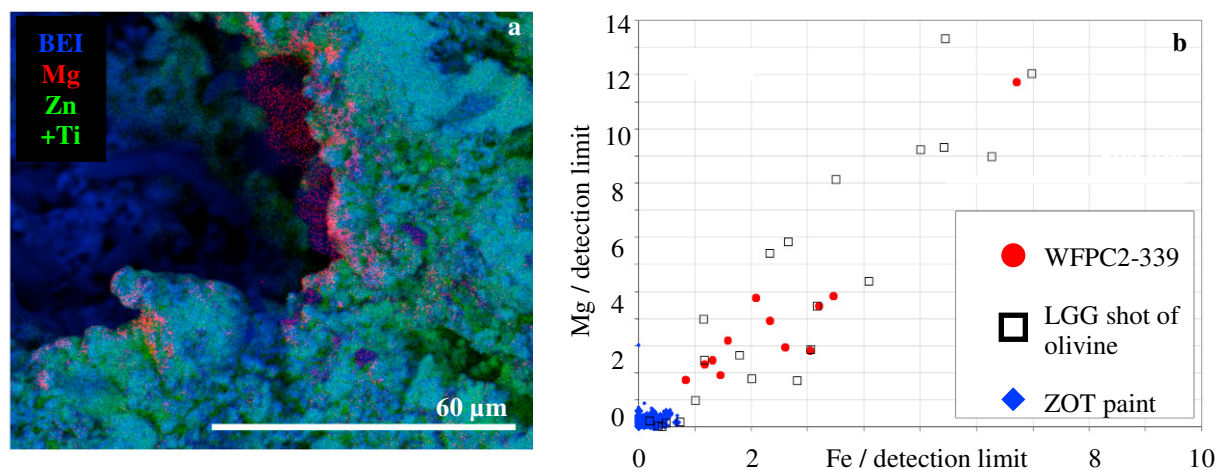

Fig. 4. Small impact WFPC2-339: a) BEI and SEM-EDX maps show Mg-rich residue concentrated in thin frozen frothy paint melt, lining the impact pit ; b) plot shows higher Mg and Fe levels in spectra of impact melt (red circles) than in clean ZOT paint (blue diamonds); and similar to residue from LGG of olivine grains (open black squares).

3.1.2 Larger impact features, exposing, penetrating and melting the alloy layer (Fig. 5).

To find subtle extraneous element signatures in larger craters on underlying Al-6061, a second type of plot was created. Frozen melt is usually dominated by alloy elements: Al, major Mg, and minor Cr and Fe. Because of variation in X-ray absorption and fluorescence at different locations in impact features, it is not wise to make direct comparison of X-ray counts across a wide energy range (e.g. apparent Fe:Al ratio is strongly affected by topography). However, coupled pairs: Mg and Al; Cr and Fe have similar X-ray energies, and are not strongly biased. To reveal the range of composition for pristine alloy (without impactor residue), Mg/Al counts were plotted against Cr/Fe for 1300 SEM-EDX point spectra and 30 areas of ~ 30 µm^2 (Fig. 5, grey, black and yellow). Individual alloy inclusions (Mg+Si 0.3%, Fe+Cr 1.8%) were also plotted (green/yellow), but their relatively low abundance in the alloy means that their individual point spectra are not easy to confuse with a cluster or trend of points given by multiple residue analyses (e.g. Fig 5, red points). Deviations from alloy composition show addition of specific types of material [6] - this method was successful in isolating impactor signatures in 27 WFPC2 features.
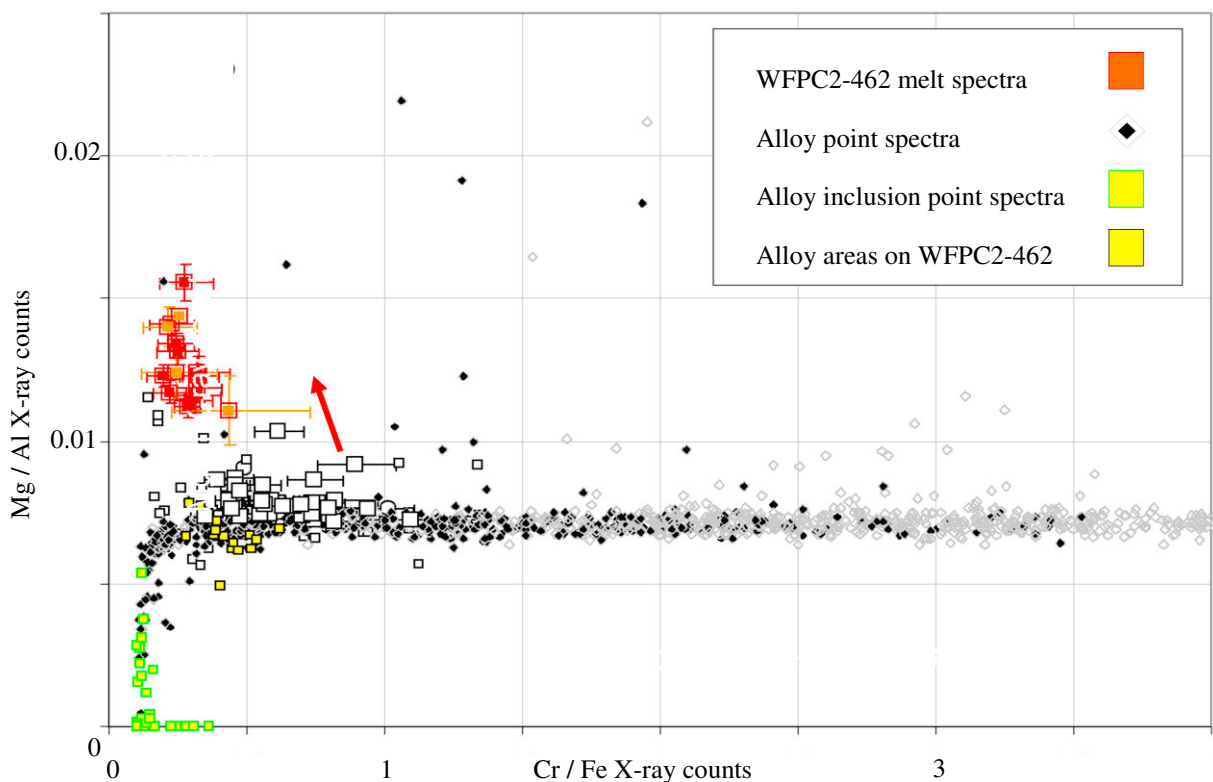

Fig. 5: Large impact crater WFPC2-462 in alloy. Plot of Mg/Al versus Cr/Fe raw X-ray peak counts in SEM-EDX spectra from melt at crater edge (orange and red) shows enrichment of Mg and Fe over pristine alloy areas (open squares from polished section standard, yellow filled squares from exposed clean alloy on sample 462) and above point spectra from polished section (diamonds, grey diamonds indicate Fe counts below detection limit convention).

4. Interpretation of impactor origins

Impactor origin was classified by sequential Decision Trees [12]. For example in Tree (a) of Fig. 6, Mg and Fe found at high levels together (without significant Al), would indicate a MM impactor (Note 3: Mg and Fe are often found together in natural silicates e.g. olivine and pyroxene [13], the most common MM components, and in natural oxides e.g. spinel - they only occur separately as major components of specific artificial alloy materials that might

contribute to OD). If there was relatively low Fe, and high Cu, Zr, Ag or rare earth elements, this would indicate specialist aerospace alloy OD impactor (Note 5, [14]). Low iron with high Mn would indicate a diagnostic 'low-iron, manganese-enriched' (LIME) MM silicate (Note 2), but low iron and low Mn could indicate either an Mg end-member MM silicate such as forsterite olivine or enstatite pyroxene (Note 3), or an unusual Mg-alloy (Note 4).

If Mg was not enriched, but Fe was present, the next tree (Fig. 6 b) was employed. Presence of high S associated with Fe ($\pm$ Ni) would suggest a MM sulfide impactor (Note 6), but in the absence of S: Cr+Ni would indicate a ferrous alloy OD particle (Note 10); Fe+Cr alone, would indicate an oxide spinel MM; whereas Fe+Ni alone, would be metallic MM (Note 7). If no other elements are detected, the residue might indicate Fe oxide, carbide or silicate MM (Note 8), or mild steel OD (Note 9).

If the detected composition did not meet any of the criteria in Tree (b), then presence of Ca was tested (Fig. 6 c); if this lead to no attribution, then the test moved to S in Tree (d) and finally to Al in Tree (e). At this point, if no other diagnostic elemental signature was found, the impactor was classified as 'unresolved'. A few (4 features) contained only elevated Fe, and could have been either MM or OD.

Given their variable but high concentration in ZOT paint, it was not possible to recognize impactor addition of K, Ti or Zn. The strong overlap of Na K X-ray lines by Zn L X-rays also precluded recognition of this element, hence OD impacts by paint pigment and reactor coolant metal could not be recognized on the WFPC2 radiator.
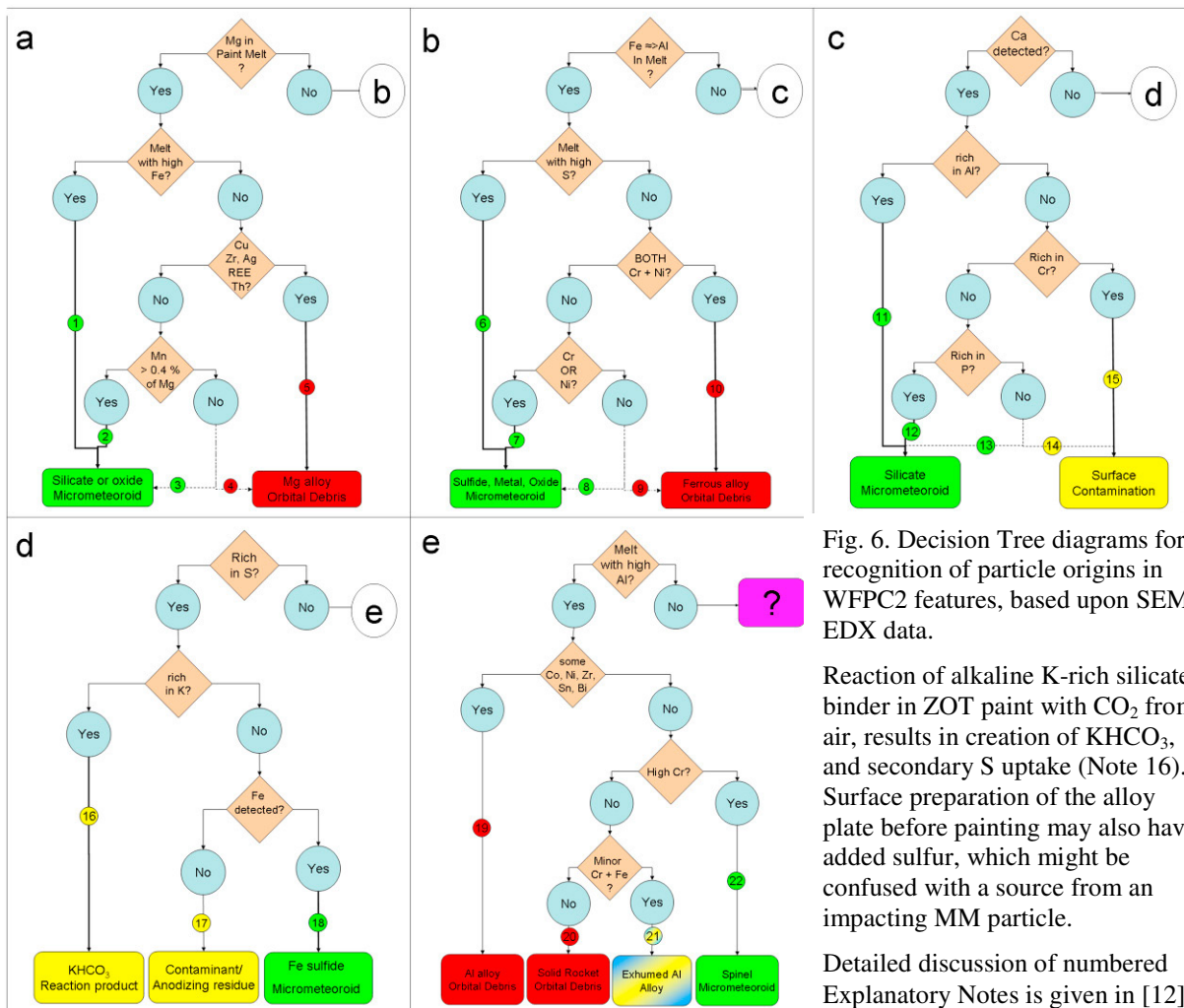

Fig. 6. Decision Tree diagrams for recognition of particle origins in WFPC2 features, based upon SEM-EDX data.

Reaction of alkaline K-rich silicate binder in ZOT paint with CO_2 from air, results in creation of $KHCO_3$, and secondary S uptake (Note 16). Surface preparation of the alloy plate before painting may also have added sulfur, which might be confused with a source from an impacting MM particle.

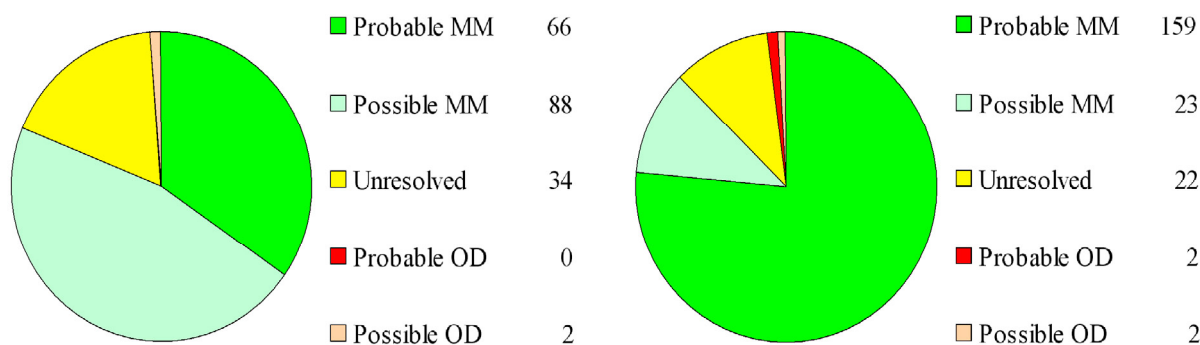Detailed discussion of numbered Explanatory Notes is given in [12].

5. Summary

Fig. 7. Proportions of impactor origins based upon analysis of particle residues: left) at NASA; right) at NHM/IBC.

In 190 WFPC2 samples examined at NASA- JSC, residues from 154 MM and 2 OD were found, but 34 features gave no definitive evidence (Fig. 7). In the UK, the 208 features examined (including cross validation samples) showed 182 MM and 4 OD residues. The 22 unresolved features included 4 that might be from either MM or OD (the extraneous signature was ambiguous as to its origin); 10 in which no diagnostic residue was detected; and 8 with impacted areas obscured by surface contamination. The higher attribution of 'probable' (as opposed to 'possible') MM status in samples examined in the UK reflects the collection of very large numbers of long-duration SEM-EDX spectra at the NHM and the use of plots like those shown in Figs. 4 and 5, along with the recognition of very low concentration residues by PIXE at the Ion Beam Centre of the University of Surrey in Guildford.

6. Discussion and Conclusions

Positive attribution of impactor origins for 86% of the WFPC2 features examined (342/398) is a considerable enhancement over results from earlier studies of LEO impacts, such as ~ 75% of impact features examined on HST solar cells [2].

The WFPC2 radiator shield clearly acted as an excellent collector of hypervelocity impact residues, especially with the porous paint layer capturing melted remains. Microanalysis of impact melt from both paint and metal layers showed that the particles were dominated by natural micrometeoroids. Most were Mg- and Fe-rich, probably silicate minerals. Comparison of the area*time product for exposure of WFPC2 in LEO (2.2m x 0.8 m x 15.5 years) to the particle flux from HST Service Mission 3B [12], suggests that the largest MM impactor on WFPC2 was probably about 230 µm in diameter [12]. Further interpretation of individual particle dimensions may be possible in future, using cratering equations from a recent experimental calibration for the WFPC2 substrate [15].

The development of high count rate and large take-off angle EDX detectors, powerful spectral de-convolution software and novel graphical plots have proven very successful in identifying particle origins for hypervelocity impactors on the complex WFPC2 radiator shield components. Similar approaches to impactor residue analysis could yield important information about particle fluxes in future studies of material returned from LEO. A critical step will lie in the use of micro-beam instruments and X-ray detectors that can acquire spectral information from across the entire complex surface shape of impact features, and full documentation of the impacted substrate before attempting isolation of an impactor signature, and subsequent attribution of particle origins.

Acknowledgements

References

[1] A. Moussi et al., Hypervelocity impacts on HST solar arrays and the debris population. Adv. Space Res. 35 (2005) 1243-1253.

[2] A. T. Kearsley et al., Impacts on Hubble Space Telescope solar arrays: discrimination between natural and man-made particles. Adv. Space Res. 35 (2005) 1254-1262.

[3] J. N. Opiela, J.-C. Liou, P.D. Anz-Meador., Micrometeoroid and Orbital Debris Impact Feature Size and Position Data Collected During the Post-Flight Survey of the Hubble Wide Field Planetary Camera 2. (2012) NASA/TP-2012-217359.

[4] P. Anz-Meador et al., Sampling and Analysis of Impact Crater Residues found on the Wide Field Planetary Camera-2 Radiator. (2013) Proc. 6th European Conf. Space Debris, ESA SP 723: s1b_anzme.pdf, CD-ROM.

[5] D. K. Ross et al., Micrometeoroid Impacts on the Hubble Space Telescope Wide Field and Planetary Camera 2: Smaller Particle Impacts. LPSC 45 (2014) #1514.

[6] A. T. Kearsley et al., Micrometeoroid Impacts on the Hubble Space Telescope Wide Field and Planetary Camera 2: Larger Particles. LPSC 45 (2014) #1722.

[7] G.A. Graham et al. Analysis of Impact Residues on Spacecraft Surfaces: Possibilities and Problems, In: Proceedings of the Third European Conference on Space Debris, ESA Special Publication 473 (2001) 197-203.

[8] F. Hörz et al., Preliminary Analysis of LDEF Instrument A0187-1 "Chemistry Of Micrometeoroids Experiment", In: Levine, A.S. (ed) LDEF—69 Months in Space First Post-Retrieval Symposium NASA Conference Publication 3134 Part 1 (1992) NASA Langley Research Center, Hampton, VA 23665-5225.

[9] A. T. Kearsley et al., Impacts on the Hubble Space Telescope Wide Field and Planetary Camera 2: Microanalysis and Recognition of Micrometeoroid Compositions. LPSC 45 (2014) #1733.

[10] J. L. Colaux et al., Micrometeoroid Impacts on the Hubble Space Telescope Wide Field and Planetary Camera 2: Ion Beam Analysis of Subtle Impactor Traces. LPSC 45 (2014) #1727.

[11] M. C. Price et al., Impacts on the Hubble Space Telescope Wide Field and Planetary Camera 2: Experimental Simulation of Micrometeoroid Capture. LPSC 45 (2014) #1466.

[12] A. T. Kearsley et al., Determination of origin for impact features on the radiator cover for the Wide Field and Planetary Camera, returned from the Hubble Space Telescope (HST) in 2009 by shuttle orbiter Atlantis during HST Service Mission 4 (HST SM-4). Final Report for ESA contract 40001105713/12/NL/GE. (2012) 88pp.

[13] A. J. Brearley, R.H. Jones, Chondritic Meteorites, In: Papike, J.J. (ed.) Planetary Materials. Reviews in Mineralogy, 36 (2000) Mineralogical Society of America.

[14] P. Lyon., New Magnesium Alloy for Aerospace and Speciality Applications. In: Luo A. A. (ed) Magnesium Technology 2004 TMS (The Minerals, Metals & Materials Society), (2004) Wiley. pp 311-315. ISBN-13: 978-0470952979; ISBN-10: 0470952970. CD-ROM.

[15] E. Christiansen. pers. comm. (March 2017).